International Journal of Scientific Research in Science and Technology
Print ISSN: 2395-6011 | Online ISSN: 2395-602X (www.ijsrst.com)
doi : https://doi.org/10.32628/IJSRST229647

Adsorption Characteristics of Some Azo Dye on Nanobiocomposite in a Column Operation

Mitali Sarkar[1*], Pankaj Sarkar[2*]

[1*]Department of Chemistry, University of Kalyani, Kalyani, West Bengal, India

[2]Department of Chemistry, Nabadwip Vidyasagar College, Nabadwip, West Bengal, India

Article Info
Volume 9, Issue 6
Page Number : 353-361

Publication Issue
November-December-2022

Article History
Accepted : 20 Nov 2022
Published : 05 Dec 2022

ABSTRACT

Unfixed dyes released from various industries directly impact on the environment quality which is quite alarming and a matter of concern. In the present study, the removal of a carcinogenic azo dye, congo red (CR), was modelled for column adsorption dynamics following batch study in aqueous solution using iron modified cellulose nanobead. The effect of process parameters has been described for both batch and column study. Adsorption capacity of CR in the batch mode and column mode was calculated to be 3.29 and 8.69 mg g^{-1} respectively. The elution of retained CR from FeCNB phase was performed using 1.0 x 10^{-1} mol dm^{-3} NaOH and the maximum elution was found to be 81.25%. The experimental data were well described by BDST model.

Keywords: Congo Red, Iron Modified Cellulose Nanobead, Batch and Column Adsorption, Elution

I. INTRODUCTION

Rapid industrialization has made a serious impact on the environment with introduction of several xenobiotic compounds. Dyes are widely used in several industrial operations and as a result huge amount of dye wastewater are introduced in the environment [1]. The presence of these compounds has become a cause of worldwide concern due to their persistence, toxicity and health hazards. It is therefore of prime necessity to control the load of such toxicants prior to discharge into receiving water bodies. Popular treatment processes include biological degradation [2-4], chemical oxidation [5-9] and adsorption [10-12] for monitoring. Considering the simplicity and ease of operation, toxic organic compounds are widely removed from aqueous waste streams by adsorption onto a solid surface via weak van der Waals forces. Separation and removal of dyes, too, by adsorption is a promising field of research. Several techniques such as AOPs [5-9], coagulation-flocculation [13-14], membrane separation [15-16], bioaccumulation [17-18], dialysis/ electrodialysis [19], reverse osmosis (RO) [20-21], ion-exchange [22], biosorption [23-24], phytoremediation [25] including adsorption [10-12] are used for dye removal. Common adsorbents for CR are mainly derived from different natural products such as biomass, agricultural waste,

rock, clay etc. In addition, nanoparticles and nanocomposites, as adsorbent show promise in removing CR from water and wastewater.

The effectiveness of iron(III) modified cellulose nanobead, the iron cellulose nanocomposite (FeCNB) in removing CR, an azo dye was studied in batch mode [26]. In continuation, the present report deals with the design, operation and performance of a fixed bed FeCNB column for removal of CR. In order to simulate the design of column operation knowledge of adsorption isotherms as well flow dynamics is considered.

II. MATERIALS AND METHODS

2.1. Materials

The chemicals and the solvents used are of Analytical grade. Congo red (CR) and cellulose powder (CS) were purchased from Merck Loba Chemie, India respectively. A stock solution (250 mg dm^{-3}) of CR was prepared using deionized water. Fe(III) nitrate (Merck, India) solution (10% w/v) was prepared and used for the synthesis of the FeCNB.

2.2. Synthesis of the nanobiocomposite, the adsorbent

The synthesis of Fe(III) loaded cellulose nanocomposite bead (FeCNB) was made in a two steps process via, synthesis of cellulose nanobead (CNB) using sol-gel technique and iron loaded cellulose nanocomposite bead (FeCNB) by impregnation of ferric nitrate (10% w/v) over CNB [26].

2.3. Batch study

In the batch adsorption process CR solution of known concentration was agitated with FeCNB in an incubator till the attainment of the equilibrium. The solution was filtered and the CR concentration in the filtrate was measured spectrophotometrically at a wave length of 498 nm. The process was optimized for dose (1.0 g), initial CR concentration (50–200 mg dm^{-3}), shaking time (5-200 min), pH (2.2-8.5) and temperature (293-313 K) of working solution [26]. The kinetic investigation was performed by withdrawing the CR solution at regular adsorption time interval.

2.3. Column study

Column dynamic experiment was performed in a down-flow manner using a perspex column (i.d. 1.3 cm, length 60.0 cm) packed with FeCNB of uniform size following the procedure of Hutchins [27]. The feed solution flow rate was controlled through a flow controller. The process was investigated for the feed flow rate (2.0-6.0 cm^3 min^{-1}), feed CR concentration (50–150 mg dm^{-3}) and FeCNB bed height (10–30 cm) in the column. The effluent was collected from the column end at regular time intervals and CR concentration was measured spectrophotometrically at a wave length of 498 nm.

III. RESULTS AND DISCUSSION

3.1. Characterization of FeCNB sample

The FeCNB sample was characterized for FT-IR spectra, SEM and associated EDAX (FEI Quanta FEG 250), FESEM (JEOL, JSM 6700 F with voltage 5.0 kV), and TEM (JEOL-JEM-2100-HR) studies. The O-H stretching, symmetrical C-H stretching, C-H bending (in plane) as well as C-O-C, C-C-O, C-C-H deformation and stretching of cellulose moiety was noticed from FTIR spectra [26]. The observed bands due to the stretching and bending vibration of Fe-O and O-Fe-O were indicated binding of Fe with cellulose [28]. The surface roughness and topography were investigated from SEM and FESEM. Presence of carbon, oxygen, iron, nitrogen, sulphur and sodium along with size distribution of particles in the nanoscale range was shown [26].

3.2. Parametric design of CR retention in a batch operation

3.2.1. Effect of operational parameters

Operational parameters such as adsorbent dose, solution pH and temperature, shaking time and speed

as well as the adsorbate concentration influence the adsorption extent in the batch process. Percent removal of the dye was increased initially with increasing adsorbent dose from 0.5 to 1.0 gdm^{-3} and thereafter became almost constant. The percent removal was increased from pH 2.0 to 6.0 and gradually decreased from pH 6.0 to 10.0. This can be explained from the point of zero charge of FeCNB (pH_{ZPC}; 7.58). The electrostatic interaction between positive surface of FeCNB and the anionic dye molecules prevails leading to increased removal at pH < 7.58. At pH > 7.58 the electrostatic repulsion between adsorbent surface and CR was increased and the extent of adsorption was found to diminish rapidly. It was found that the equilibrium reached in 90 min and further increase in contact time did not change the extent of adsorption. The percent removal was found to be 94.34 and 89.80% for the initial concentration of 50 and 200 $mgdm^{-3}$, respectively. With increase in shaking speed from 50 to 100 spm, percent removal was increased from 51.44 to 89.61% corresponding to dye solution of 200 mg dm^{-3}, and from 65.04 to 94.23% corresponding to dye solution of 50 mg dm^{-3}. The percent removal was decreased from 94.23 to 89.61% with an increase in initial dye concentration from 50 to 200 mg dm^{-3} at 303 K. With increase of solution temperature the extent of CR adsorption was increased from 88.58 to 95.48 % corresponding to initial CR concentration of 100 mg dm^{-3}.

3.2.2. Adsorption equilibrium study

Study of the adsorption isotherm reveals the feasibility criterion of the adsorption process. The isotherm models tested are Langmuir, Freundlich, Temkin and Sips. Fig. 1 demonstrates the equilibrium isotherm corresponding to linerized Langmuir, Freundlich, Temkin and Sips models. The applicability of a particular isotherm model was assessed from R^2 (regression coefficient) and SE (standard error of estimate) values. The higher R^2 and lower SE suggest the Langmuir model as the most fitted one. The adsorption isotherm characteristics are presented in Table 1. The thermodynamic parameters such as ΔG^0, ΔH^0 and ΔS^0 are evaluated and presented in Table 2.

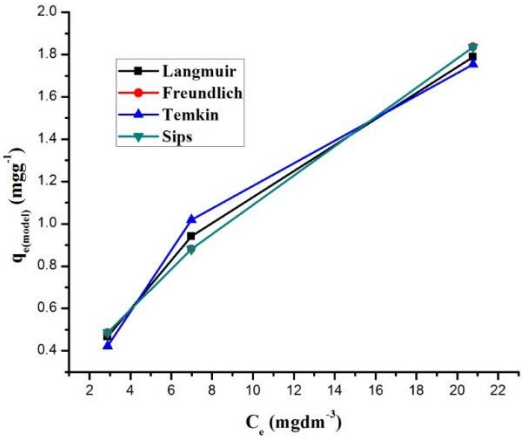

Fig. 1: Plot of model q_e against C_e of different isotherm models

Table 1: Isotherm characteristics and related linear equations:

Isotherm	Equation*	R^2	SE
Langmuir	$\frac{C_e}{q_e} = \frac{1}{q_0.b} + \frac{C_e}{q_0}$ [30]	0.9993	0.1055
Freundlich	$\ln q_e = \ln K_F + \frac{1}{n}\ln C_e$ [31]	0.9951	0.0665
Temkin	$q_e = \left(\frac{RT}{B_T}\right)\ln A_T + \left(\frac{RT}{B_T}\right)\ln C_e$ [32]	0.9873	0.1082
Sips	$\ln\left(\frac{K_s}{q_e}\right) = -\beta_s \ln C_e + \ln(A_s)$ [33]	0.9950	0.0665

*C_e (mg dm^{-3}): equilibrium concentration of adsorbate, q_e (mg g^{-1}): amount of adsorbate, b (dm^3 mg^{-1}): Langmuir adsorption constants related to energy, q_0 (mg g^{-1}): adsorption capacity, K_F (gm g^{-1}): Freundlich constant, R: Universal gas constant, T (K): temperature at which the adsorption process is performed, A_T (dm^3 mg^{-1}): adsorption capacity, B_T (J mol^{-1}): heat of adsorption, K_s (dm^3 g^{-1}): Sips isotherm

constant, β_s: Sips isotherm model exponent and A_S ($dm^3\,mg^{-1}$): Sips isotherm model constant

Table 2: Thermodynamic parameters and the related equations

Thermodynamic	Equation*	-ΔG⁰ (KJ mol⁻¹)	ΔH⁰ (KJ mol⁻¹)	ΔS⁰ (KJ mol⁻¹K⁻¹)
Gibb's	$\Delta G^0 = \Delta H^0 - T\Delta S^0$ [34]	6.311	38.23	0.147
van't Hoff	$R\ln K_C = \Delta S^0 - \frac{\Delta H^0}{T}$ [34]			

*ΔG^0: Gibb's free energy, ΔS^0: change in entropy, ΔH^0: change in enthalpy, R (J mol K^{-1}): Universal gas constant, T(K) = temperature in Kelvin scale and K_C is the equilibrium constant of the process.

3.2.3. Adsorption Kinetic study

In order to determine the rate of adsorption and plausible mechanism of CR-FeCNB interaction, pseudo-first-order and pseudo-second order kinetic models were tested. The model kinetic characteristics are presented in Table 3. The validity of the particular kinetic model was tested with R^2 and SE values. The higher R^2 and lower SE favour the Pseudo-second-order kinetic model

Table 3: Kinetic characteristics and the related linear equations

Kinetics	Equation*	R^2	SE
Pseudo-first-order	$\ln(q_e - q_t) = \ln q_e - k_1 t$ [35]	0.9794	0.6520
Pseudo-second-order	$\frac{t}{q_t} = \frac{1}{k_2 q_e^2} + \frac{t}{q_e}$ [35]	0.9982	1.016

*q_t (mgg^{-1}): amount of solute adsorbed on the surface of adsorbent at time 't', k_1: pseudo-first-order rate constant, q_e (mg g^{-1}): amount of dye adsorbed at equilibrium, k_2 (g mg^{-1} min^{-1}): pseudo-second-order rate constant

3.3. Parametric design of CR adsorption in a column operation

Adsorption isotherm, being a batch equilibrium test, however, fails to simulate or predict dynamic performance during continuous flow movement. The most important deficiency is the lack of a predictable contact time necessary to achieve the equilibrium capacity in a granular bed. In order to design the operation in a fixed bed column as well as to dictate the flow dynamics the breakthrough curve is constructed.

For the retention CR solution of known concentration and pH was continuously fed at the top of the column bed at a fixed flow rate. A plot of C_t/C_0 against time or the volume of effluent yielded the breakthrough curve. It is assumed that during solute retention on the FeCNB bed CR mass transfer occurs by convection only, no radial and axial dispersions occur, the flow pattern is ideal plug flow and no chemical reaction occurs in the column [36-37].

Retention of CR in the column occurs as equilibrium is established. With progress of time (t) the upper part of the column becomes saturated with incoming CR, in the intermediate zone CR is found in solution as well as on FeCNB surface with any CR still to reach the lower part of the column. In the intermediate interaction zone, the concentration (C) of CR retained is different at different bed or the distance (d) from the top of the column bed. The ratio C_t/C_0 is a function of d at a given t. The interaction zone moves downwards as primary adsorption zone following the mass balance concept. Finally, the interaction zone to reach end of the column at the breakthrough point (t_b) and CR is first detected in the column end. At the exhaustion point (t_{ex}) the total bed became exhausted. The shape of the breakthrough curve in the column operation is largely dependent on the type of adsorption isotherm governing the static equilibrium [36]. The

performance of the column is expressed as the column capacity and was compared with that from batch operation.

3.3.1. Effect of operational parameters

The operation and performance of a column as is influenced by several operational parameters like the bed height, volume, concentration and flow rate of the feed solution, the optimization of such variables was made.

3.3.1.1. Effect of feed CR concentration

CR retention on the FeCNB column was investigated with different CR concentrations, viz. 50, 100 and 150 mg dm^{-3}. Sharp breakthrough curve was obtained at higher feed CR concentration. The breakthrough time decreases as the feed CR concentration increases. The percent adsorption lies in the range between 35.47 and 70.32 % and found to increase with feed CR concentration (Table 4).

3.3.1.2. Effect of flow rate of feed CR solution

The effect of flow rate of the feed CR solution was studied for a fixed CR concentration (100 mg dm^{-3}) and FeCNB bed height (20 cm). It is found that the column capacity does not change up to a flow rate (F) of 7.0 cm^3 min^{-1} even for the highest concentration studied. However, in subsequent studies a flow rate of 4.0 cm^3 min^{-1} was maintained. At a lower flow rate due to adequate interaction time adsorption was expected to be very efficient and with progress of solution movement CR retention gradually decreases. With increase of flow rate the breakthrough curve becomes steeper. The breakthrough time and adsorbed CR concentration decreases (Table 4) due to the shorter residence time of CR in column.

3.3.1.3. Effect of FeCNB bed height

In order to study the effect of bed height on CR retention, FeCNB column of three different bed depths, viz. 10, 20 and 30 cm were taken. CR solution of fixed concentration (100 mg dm^{-3}) was passed through the individual column at a fixed flow rate of 4.0 cm^3 min^{-1}. The experimental study revealed that the percent adsorption (P) increases with increasing bed height and initial concentration but decreases with flow rate (Table 4).

Table 4: Column characteristics of CR adsorption

d (cm)	F (cm^3 min^{-1})	C_0 (mg dm^{-3})	t_b (min)	t_{ex} (min)	% P
10	4	100	42	606	55.58
20	4	100	50	725	55.62
30	4	100	57	825	61.24
20	2	100	100	1100	58.41
20	6	100	47	550	52.00
20	4	50	28	550	35.47
20	4	150	97	1000	70.32

*d (cm): bed depth, F (cm^3 min^{-1}) flow rate, C_0 (mg dm^{-3}): initial CR concentration, t_b (min): breakthrough time, t_{ex} (min): bed exhaust time, P: Column adsorption (%) of CR

3.3.2. Breakthrough service time model

Breakthrough service time (BDST) model is used to predict the column performance for any bed length. A linear relation between bed depth and service time is given by Eq. 1 [27].

$$t = \frac{N_0 Z}{C_0 \nu} - \frac{1}{K_a C_0} \ln\left(\frac{C_0}{C_b} - 1\right) \quad (1)$$

Where C_0 is the initial dye concentration ($mgdm^{-3}$), N_0 is the adsorption capacity of bed ($mgdm^{-3}$), ν is the linear velocity (cm h^{-1}), C_b is the breakthrough CR concentration ($mgdm^{-3}$) and K_a is the rate constant ($dm^3mg^{-1}h^{-1}$).

A plot of service time against bed depth, following the above model of Hutchins gives a straight line (Fig. 2). The high regression values (R^2 = 0.9985) of the linear plot indicates the validity of BDST

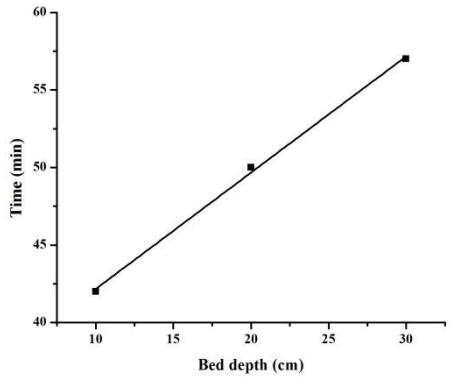

Fig. 2: Linear plot of service time against bed depth

3.4. Adsorption performance evaluation in batch and column mode

Adsorption capacity of CR in the batch mode and column mode is calculated to be 3.29 and 8.69 mg g^{-1}, respectively, indicating that column capacity is higher than the batch capacity for the CR–FeCNB system. Thus, column operation is preferred to the batch operation.

3.5. Elution study

Elution of the retained CR from the FeCNB phase was tested with different eluting agents such as ethanol, methanol, 1:1 ethanol/H_2O, 1:1 methanol/H_2O and sodium hydroxide solution. It was found that the maximum elution of retained CR from FeCNB phase was achieved using sodium hydroxide solution as the eluting agent. The elution process was also performed using different concentrations of sodium hydroxide. A constant flow rate of 3.0 cm^3 min^{-1} was maintained throughout the operation. It is found that a maximum of 81.25% of retained CR was eluted with1.0 x 10^{-1} mol dm^{-3} NaOH solution.

3.6. Effectiveness of the column operation

In order to find the effectiveness of the column the operation is repeated for a number of times and the capacity after each cycle was evaluated. In a typical set with initial CR concentration of 100 mg dm^{-3} and bed height 20 cm, the retention–elution (NaOH:1.0 x 10^{-1} mol dm^{-3}) process was repeated for five times. It is found that column capacity decreases with cycle number although remains within 66.8%. The experimental column capacity (8.69 mg g^{-1}) is compared with theoretical breakthrough capacity (8.75 mg g^{-1}) as well as the CR recovery (7.06 mg g^{-1}) through elution.

IV. CONCLUSIONS

FeCNB, the nanobiocomposite is found to be a suitable adsorbent for the removal of CR from aqueous sample. The equilibrium behaviour of the adsorption was represented by Langmuir and Freundlich isotherm model. The thermodynamic constants estimate that CR removal on FeCNB is feasible and spontaneous.

The mass balance concept is applied to predict the behaviour of solution movement through the column. The nature of breakthrough curve is influenced by the flow rate, column bed height, adsorption capacity and adsorption rate. The formation of primary adsorption zone is predicted and characterized by different secondary parameters. The column capacity is found higher compared to the batch capacity. The retained CR can be eluted with NaOH solution (1.0 x 10^{-1} mol dm^{-3}).

V. ACKNOWLEDGEMENTS

The authors gratefully acknowledge the facilities provided by DST-FIST, New Delhi, Government of India, to the Department of Chemistry, Kalyani University. Sincere thanks are due to IACS, Kolkata and SNBNCBS, Kolkata for the physico-chemical analysis of the adsorbent.

VI. REFERENCES

[1]. Paździor, K., Bilińska, L., & Ledakowicz, S. (2019). A review of the existing and emerging technologies in the combination of AOPs and biological processes in industrial textile

wastewater treatment. Chemical Engineering Journal, 376, 120597.

[2]. Sriram, N., Reetha, D., & Saranraj, P. (2013). Biological degradation of reactive dyes by using bacteria isolated from dye effluent contaminated soil. Middle–East Journal of Scientific Research, 17(12), 1695-1700.

[3]. Mishra, S., Nayak, J. K., & Maiti, A. (2020). Bacteria-mediated bio-degradation of reactive azo dyes coupled with bio-energy generation from model wastewater. Clean Technologies and Environmental Policy, 22(3), 651-667.

[4]. Ikram, M., Naeem, M., Zahoor, M., Hanafiah, M. M., Oyekanmi, A. A., Ullah, R., ... & Gulfam, N. (2022). Biological degradation of the azo dye basic orange 2 by Escherichia coli: A sustainable and ecofriendly approach for the treatment of textile wastewater. Water, 14(13), 2063.

[5]. Nawaz, S., Siddique, M., Khan, R., Riaz, N., Waheed, U., Shahzadi, I., & Ali, A. (2022). Ultrasound-assisted hydrogen peroxide and iron sulfate mediated Fenton process as an efficient advanced oxidation process for the removal of congo red dye. Polish Journal of Environmental Studies, 31(3), 2749-2761.

[6]. Saleh, R., & Taufik, A. (2019). Degradation of methylene blue and congo-red dyes using Fenton, photo-Fenton, sono-Fenton, and sonophoto-Fenton methods in the presence of iron (II, III) oxide/zinc oxide/graphene (Fe3O4/ZnO/graphene) composites. Separation and Purification Technology, 210, 563-573.

[7]. Solano, A. M. S., Garcia-Segura, S., Martinez-Huitle, C. A., & Brillas, E. (2015). Degradation of acidic aqueous solutions of the diazo dye Congo Red by photo-assisted electrochemical processes based on Fenton's reaction chemistry. Applied Catalysis B: Environmental, 168, 559-571.

[8]. Khadhraoui, M., Trabelsi, H., Ksibi, M., Bouguerra, S., & Elleuch, B. (2009). Discoloration and detoxicification of a Congo red dye solution by means of ozone treatment for a possible water reuse. Journal of Hazardous Materials, 161(2-3), 974-981.

[9]. Gharbani, P., Tabatabaii, S. M., & Mehrizad, A. (2008). Removal of Congo red from textile wastewater by ozonation. International Journal of Environmental Science & Technology, 5(4), 495-500.

[10]. Eltaweil, A. S., Elshishini, H. M., Ghatass, Z. F., & Elsubruiti, G. M. (2021). Ultra-high adsorption capacity and selective removal of Congo red over aminated graphene oxide modified Mn-doped UiO-66 MOF. Powder Technology, 379, 407-416.

[11]. Xie, J., Yamaguchi, T., & Oh, J. M. (2021). Synthesis of a mesoporous Mg–Al–mixed metal oxide with P123 template for effective removal of Congo red via aggregation-driven adsorption. Journal of Solid State Chemistry, 293, 121758.

[12]. Al-Salihi, S., Jasim, A. M., Fidalgo, M. M., & Xing, Y. (2022). Removal of Congo red dyes from aqueous solutions by porous γ-alumina nanoshells. Chemosphere, 286, 131769.

[13]. Gadekar, M. R., & Ahammed, M. M. (2016). Coagulation/flocculation process for dye removal using water treatment residuals: modelling through artificial neural networks. Desalination and Water Treatment, 57(55), 26392-26400.

[14]. Moghaddam, S. S., Moghaddam, M. A., & Arami, M. (2010). Coagulation/flocculation process for dye removal using sludge from water treatment plant: optimization through response surface methodology. Journal of hazardous materials, 175(1-3), 651-657.

[15]. Chen, H., Zhang, Y. J., He, P. Y., Li, C. J., & Li, H. (2020). Coupling of self-supporting geopolymer membrane with intercepted Cr (III) for dye wastewater treatment by hybrid photocatalysis and membrane separation. Applied Surface Science, 515, 146024.

[16]. Mo, J. H., Lee, Y. H., Kim, J., Jeong, J. Y., & Jegal, J. (2008). Treatment of dye aqueous solutions using nanofiltration polyamide composite membranes for the dye wastewater reuse. Dyes and Pigments, 76(2), 429-434.

[17]. Aksu, Z. (2003). Reactive dye bioaccumulation by Saccharomyces cerevisiae. Process Biochemistry, 38(10), 1437-1444.

[18]. Kaushik, P., & Malik, A. (2013). Comparative performance evaluation of Aspergillus lentulus for dye removal through bioaccumulation and biosorption. Environmental Science and Pollution Research, 20(5), 2882-2892.

[19]. Sivakumar, D., Shankar, D., Kandaswamy, A. N., & Ammaiappan, M. (2014). Role of electro-dialysis and electro-dialysis cum adsorption for chromium (VI) reduction. Pollution Research, 33, 547-552.

[20]. Nataraj, S. K., Hosamani, K. M., & Aminabhavi, T. M. (2009). Nanofiltration and reverse osmosis thin film composite membrane module for the removal of dye and salts from the simulated mixtures. Desalination, 249(1), 12-17.

[21]. Abid, M. F., Zablouk, M. A., & Abid-Alameer, A. M. (2012). Experimental study of dye removal from industrial wastewater by membrane technologies of reverse osmosis and nanofiltration. Iranian Journal of Environmental Health science & Engineering, 9(1), 1-9.

[22]. Joseph, J., Radhakrishnan, R. C., Johnson, J. K., Joy, S. P., & Thomas, J. (2020). Ion-exchange mediated removal of cationic dye-stuffs from water using ammonium phosphomolybdate. Materials Chemistry and Physics, 242, 122488.

[23]. Robinson, T., Chandran, B., & Nigam, P. (2002). Removal of dyes from a synthetic textile dye effluent by biosorption on apple pomace and wheat straw. Water Research, 36(11), 2824-2830.

[24]. Gong, R., Ding, Y., Li, M., Yang, C., Liu, H., & Sun, Y. (2005). Utilization of powdered peanut hull as biosorbent for removal of anionic dyes from aqueous solution. Dyes and Pigments, 64(3), 187-192.

[25]. Bharathiraja, B., Jayamuthunagai, J., Praveenkumar, R., & Iyyappan, J. (2018). Phytoremediation techniques for the removal of dye in wastewater. In Bioremediation: applications for environmental protection and management (pp. 243-252). Springer, Singapore.

[26]. Sarkar, P., Sarkar, S., Santra, D., Denrah, S., & Sarkar, M. (2022). Study of Isotherm and Kinetics for Remediation of Congo Red Using Nanocomposite Bead. Fine Chemical Engineering, 133-155.

[27]. Hutchins, R.A., 1973. New method simplifies design of activated carbon systems. Chemical Engineering, 80, 133–138.

[28]. Stoica-Guzun, A., Stroescu, M., Jinga, S. I., Mihalache, N., Botez, A., Matei, C., ... & Ionita, V. (2016). Box-Behnken experimental design for chromium (VI) ions removal by bacterial cellulose-magnetite composites. International Journal of Biological Macromolecules, 91, 1062-1072.

[29]. Zhang, Z. H., Zhang, J. L., Liu, J. M., Xiong, Z. H., & Chen, X. (2016). Selective and competitive adsorption of azo dyes on the metal–organic framework ZIF-67. Water, Air, & Soil Pollution, 227(12), 1-12.

[30]. Sarkar, S., & Sarkar, M. (2019). Ultrasound assisted batch operation for the adsorption of hexavalent chromium onto engineered nanobiocomposite. Heliyon, 5(4), e01491.

[31]. Sarkar, M., Sarkar, P., Sarkar, S., & Denrah, S. (2021). Optimization and Feasibility of Alizarin Red S Retention on Iron-Loaded Cellulose Nanocomposite Bead. Nanoarchitectonics, 39-60.

[32]. Sarkar, M., & Sarkar, S. (2017). Adsorption of Cr (VI) on Iron (III) cellulose nanocomposite bead. Environmental Processes, 4(4), 851-871.

[33]. Ayawei, N., Ebelegi, A.N., & Wankasi, D. (2017). Modelling and interpretation of adsorption isotherms. Journal of Chemistry, 2017.

[34]. Sarkar, M., Santra, D., Denrah, S., Sarkar, S., & Sarkar, P. (2021). Study on the Efficiency of Metal Modified Bio–Nanocomposite Bead for Removal via Retention of Some Anthraquinone Dye. Challenges and Advances in Chemical Science Vol. 3, 60-78.

[35]. Santra, D., & Sarkar, M. (2016). Optimization of process variables and mechanism of arsenic (V) adsorption onto cellulose nanocomposite. Journal of Molecular Liquids, 224, 290-302.

[36]. Sarkar, M., Banerjee, A., Pramanick, P. P., & Sarkar, A. R. (2007). Design and operation of fixed bed laterite column for the removal of fluoride from water. Chemical Engineering Journal, 131(1-3), 329-335.

[37]. Hethnawi, A., Nassar, N. N., Manasrah, A. D., & Vitale, G. (2017). Polyethylenimine-functionalized pyroxene nanoparticles embedded on Diatomite for adsorptive removal of dye from textile wastewater in a fixed-bed column. Chemical Engineering Journal, 320, 389-404.

Cite this article as :

Mitali Sarkar, Pankaj Sarkar, "Adsorption Characteristics of Some Azo Dye on Nanobiocomposite in a Column Operation", International Journal of Scientific Research in Science and Technology (IJSRST), Online ISSN : 2395-602X, Print ISSN : 2395-6011, Volume 9 Issue 6, pp. 353-361, November-December 2022. Available at doi : https://doi.org/10.32628/IJSRST229647
Journal URL : https://ijsrst.com/IJSRST229647